MRL/MpJ mice produce more oocytes and exhibit impaired fertilisation and accelerated luteinisation after superovulation treatment

Marina Hosotani[A], *Osamu Ichii*[A], *Teppei Nakamura*[A,B], *Md Abdul Masum*[A], *Yuki Otani*[A], *Saori Otsuka-Kanazawa*[A], *Yaser Hosny Ali Elewa*[A] *and Yasuhiro Kon*[A,C]

[A]Laboratory of Anatomy, Division of Basic Veterinary Sciences, Faculty of Veterinary Medicine, Hokkaido University, Kita 18, Nishi 9, Kita-Ku, Sapporo, Hokkaido 060-0818, Japan.

[B]Section of Biological Safety Research, Chitose Laboratory, Japan Food Research Laboratories, Bunkyo 2–3, Chitose, Hokkaido 066-0052, Japan.

[C]Corresponding author. Email: y-kon@vetmed.hokudai.ac.jp

MRL/MpJ mice exhibit distinct phenotypes in several biological processes, including wound healing. Herein we report two unique phenotypes in the female reproductive system of MRL/MpJ mice that affect ovulation and luteinisation. We found that superovulation treatment resulted in the production of significantly more oocytes in MRL/MpJ than C57BL/6 mice (71.0 ± 13.4 vs 26.8 ± 2.8 respectively). However, no exon mutations were detected in genes coding for female reproductive hormones or their receptors in MRL/MpJ mice. In addition, the fertilisation rate was lower for ovulated oocytes from MRL/MpJ than C57BL/6 mice, with most of the fertilised oocytes showing abnormal morphology, characterised by deformation and cytolysis. Histological tracing of luteinisation showed that MRL/MpJ mice formed corpora lutea within 36 h after ovulation, whereas C57BL/6 mice were still at the corpora haemorrhagica formation stage after 36 h. The balance between the expression of matrix metalloproteinases and their tissue inhibitors shifted towards the former earlier after ovulation in MRL/MpJ than C57BL/6 mice. This result indicates a possible link between accelerated extracellular matrix remodelling in the ovulated or ruptured follicles and luteinisation in MRL/MpJ mice. Together,

these findings reveal novel phenotypes in MRL/MpJ mice that provide novel insights into reproductive biology.

Additional keywords: Ovary, histology, *in vitro* fertilisation, extracellular matrix

We report two novel and unique phenotypes of MRL/MpJ mice in the female reproductive function. Superovulation treatment resulted in the production of significantly more oocytes with lower quality, and the faster luteinisation of ovulated follicles in MRL/MpJ than C57BL/6 mice. Our results provide novel insights into the effects of artificial ovulation on oocytes and ovaries in mice.

Introduction

The Murphy Roths Large (MRL)/MpJ mouse strain was established by selective interbreeding of the C57BL/6 (0.3%), C3H (12.1%), AKR (12.6%) and LG (75%) strains (Heydemann 2012). MRL/MpJ is well known as a strain that exhibits a unique tissue repair response to various injuries (Heydemann 2012). For example, in MRL/MpJ mice, ear punches approximately 2 mm in diameter (Clark *et al*. 1998) or heart injuries induced with a cryoprobe (Leferovich *et al*. 2001) repair without scarring or fibrosis. In addition, after Caesarean delivery, uterine wound healing in MRL/MpJ mice showed histological, mitotic and functional differences compared with the C57BL/6 strain (Buhimschi *et al*. 2010). In the kidney, an organ that does not regenerate, fibrotic activity was lower and calcification was increased after acute injury in MRL/MpJ than C57BL/6 mice (Shiozuru *et al*. 2016).

The MRL/MpJ-Fas$^{lpr/lpr}$ strain, which bears the lymphoproliferation mutation (*lpr*) in the Fas cell surface death receptor (*Fas*) gene, exhibits severe autoimmune disease symptoms that are

similar to human systemic lupus erythematosus (Santiago-Raber *et al*. 2004). Although MRL/MpJ mice have been used as healthy controls for MRL/MpJ-Fas$^{lpr/lpr}$ mice inpathological studies, they also show a propensity for autoimmune diseases (Heydemann 2012). Previously, we clarified the crucial contribution of the telomeric region of chromosome 1 in the pathogenesis of autoantibody production, splenomegaly and glomerulonephritis in MRL/MpJ mice (Ichii *et al*. 2008). We also identified several genetic loci associated with reproductive system phenotypes in this strain, such as the emergence of ovarian cysts (Kon *et al*. 2007), numerous ovarian mast cells (Nakamura *et al*. 2014), testicular oocytes (Otsuka *et al*. 2008) and spermatocyte apoptosis (Kon and Endoh 2000). Thus, MRL/MpJ mice show unique phenotypes not only with regard to tissue repair and autoimmune disease capacity, but also in the reproductive system.

Previously, we established a novel method to evaluate the pick-up efficiency of ovulated oocytes in mouse oviducts (Hosotani *et al*. 2018). Using this method, we found that MRL/MpJ mice subjected to hormonal superovulation produced a markedly larger number of cumulus–oocyte complexes (COCs) than did C57BL/6 mice at 3 months of age (Hosotani *et al*. 2018). Surprisingly, the number of COCs in the ampulla of oviducts exceeded the number of ‘ovulated oocytes’ in the ovaries of MRL/MpJ mice, as determined histologically by counting the total number of ruptured follicles, corpora haemorrhagica and the follicular antrum containing no oocytes. These results suggest that the oocyte pick-up rate in MRL/MpJ mice was over 100% (Hosotani *et al*. 2018). Therefore, we hypothesised that these unique ovarian phenotypes of MRL/MpJ mice may be due to a high sensitivity to superovulation treatment and/or faster luteinisation. Indeed, in support of the latter hypothesis, the sum of the histological number of ovulated oocytes and corpora lutea (CL) was comparable to the number of COCs in the ampulla of oviducts from MRL/MpJ mice (Hosotani *et al*. 2018).

In the present study, to investigate these hypotheses and the functional implications of the phenotypes found in the MRL/MpJ strain, we evaluated the ovulation, luteinisation and fertilisation rates of ovulated oocytes in MRL/MpJ mice. The induction of ovulation or superovulation is an important technique in human and veterinary reproductive medicine. Our results provide novel insights into the effects of artificial ovulation on oocytes and ovaries in mice.

Materials and methods

Animals

Animal experimentation was approved by the Institutional Animal Care and Use Committee of the Graduate School of Veterinary Medicine, Hokkaido University (Approval no. 13-0031). Experimental animals were handled in accordance with the Guide for the Care and Use of Laboratory Animals, Graduate School of Veterinary Medicine, Hokkaido University (approved by the Association for Assessment and Accreditation of Laboratory Animal Care International). Male C57BL/6N, female C57BL/6N and female MRL/MpJ mice (3 months old) were obtained from Japan SLC. Mice were group housed in plastic cages at 18–26°C under a 12-h light–dark cycle, and had free access to water and a commercial diet. All mice were killed by cutting the carotid artery or by cervical dislocation under deep anaesthesia using a mixture of medetomidine (0.3 mg kg^{-1}), midazolam (4 mg kg^{-1}) and butorphanol (5 mg kg^{-1}).

IVF for the fertilisation rate assay

IVF was conducted according to the manuals supplied by the Center for Animal Resources and Development, Kumamoto University (Takeo *et al*. 2008; Takeo and Nakagata 2010, 2011).

Collection of spermatozoa

Spermatozoa were obtained from the cauda epididymides of a male C57BL/6N mouse, resuspended in a dish containing 100 µL FERTIUP Mouse Sperm Preincubation Medium (KYUDO), covered with paraffin oil and incubated for 1 h at 37°C with 5% CO_2 in air.

Collection of oocytes

For superovulation treatment, pregnant mare's serum gonadotrophin (PMSG; ASKA Animal Health) was injected into C57BL/6N (n = 5) and MRL/MpJ (n = 5) mice (200 µL of 37.5 IU mL^{-1}, i.p., per mouse). Forty-eight hours after PMSG injection, mice were injected with 200 µL of 37.5 IU mL^{-1}, i.p., human chorionic gonadotropin (hCG; ASKA Animal Health) per mouse. Mice were killed 24 h after hCG injection. Intact COCs were released from the excised oviduct into 200 µL CARD MEDIUM (KYUDO), covered with paraffin oil and incubated for 30–60 min at 37°C with 5% CO_2 in air before insemination.

Insemination

After preincubation as described above, the sperm suspensions were added to a drop of CARD MEDIUM containing COCs and incubated for 24 h at 37°C with 5% CO_2 in air. The final concentration of motile spermatozoa in the fertilisation medium was 400–800 spermatozoa μL^{-1}.

The embryos obtained were counted and classified into four categories according to morphological features: fertilised embryos, unfertilised embryos, abnormal cleavage embryos and dead embryos. The number of embryos in each category was determined under a stereoscopic microscope. The fertilisation rate was calculated as follows:

Fertilisation rate (%) = 100 × no. fertilised oocytes/(total no. fertilised and unfertilised oocytes)

Oocyte counts under a natural oestrous cycle and after PMSG or hCG injection

The first group of female mice was mated with male mice in the evening. The next day, female mice (n = 5) with a vaginal plug were killed. The second group (n = 4) were injected with PMSG (200 μL of 37.5 IU mL^{-1}, i.p., per mouse) and killed 24 h after injection. The third group (n = 4) were injected with hCG (200 μL of 37.5 IU mL^{-1}, i.p., per mouse) at oestrus, which was determined by vaginal smear, and were killed 24 h after injection. COCs in the oviducts were extracted by oviductal perfusion with 0.01 M phosphate-buffered saline and the number determined under a stereoscopic microscope.

Next-generation exome sequencing

Genomic DNA was isolated from the kidneys of C57BL/6N and MRL/MpJ mice with a DNeasy kit (Qiagen). Exome capture was performed using Sureselect XT Mouse All Exon kit (Agilent Technologies). Whole-exome sequencing was performed on a HiSeq2000 machine (Illumina). The mouse mm10 assembly downloaded from the University of California Santa Cruz (UCSC; http://genome.ucsc.edu/, accessed 13 Aug 2018) was used as the reference genome for sequence alignment. Reads were mapped using Burrows–Wheeler Aligner (BWA) version 0.5.9 (http://bio-bwa.sourceforge.net/, accessed 13 Aug 2018). Single nucleotide variants (SNVs) and small insertions/deletions were identified using SAMtools version 0.1.18 (http://samtools.sourceforge.net/, accessed 13 Aug 2018). We hypothesised that mutations in genes associated with female hormones or their receptors may contribute to the high sensitivity of MRL/MpJ mice to hCG. Therefore, we compared the exome sequences of the following genes between the two strains: inhibin alpha (*Inha*), inhibin beta-B (*Inhbb*), follicle stimulating hormone beta (*Fshb*), activin A receptor, type 1 (*Acvr1*), activin receptor IIA (*Acvr2a*), activin receptor IIB (*Acvr2b*), luteinising hormone beta (*Lhb*), inhibin beta-A (*Inhba*), gonadotropin releasing hormone 1 (*Gnrh1*), luteinising hormone/choriogonadotrophin receptor (*Lhcgr*),

follicle stimulating hormone receptor (*Fshr*), oestrogen receptor 1 (*Esr1*), oestrogen receptor 2 (*Esr2*) and progesterone receptor (*Pgr*).

Histological analysis of luteinisation in superovulated mice

Mice were either injected intraperitoneally with PMSG (200 µL of 37.5 IU mL^{-1} per animal) followed 48 h later by hCG (200 µL of 37.5 IU mL^{-1} per animal) or had their ovaries removed. The hCG injection time point 48 h after the administration of PMSG was considered as 12 h before ovulation (or –12 h postovulation (h.p.o.); $n = 4$), with ovaries collected 72 h (12 h.p.o.; $n = 6$), 78 h (18 h.p.o.; $n = 4$) and 96 h (36 h.p.o.; $n = 4$) later (Fig. 1). The ovaries were fixed with 4% paraformaldehyde at 4°C overnight, embedded in paraffin and cut into 10-µm serial sections. Using serial hematoxylin–eosin (HE)-stained sections, the number of antral follicles, ruptured follicles, corpora haemorrhagica and CL was counted manually by histological observation, as described previously (Hosotani *et al*. 2018).

The ratio of the maximum to minimum diameter of oocytes contained in antral follicles was defined as the ‘oocyte aspect ratio’ and calculated on serial sections of superovulated ovaries at –12 h.p.o. Serial sections clearly showing the nucleolus were selected for this analysis. Four serial sections of ovaries were used and 13–15 oocytes from C57BL/6N mice and 40–61 oocytes from MRL/MpJ mice were analysed in each ovary to determine the oocyte aspect ratio.

Reverse transcription and quantitative real-time polymerase chain reaction

Total RNA from ovaries of C57BL/6 and MRL/MpJ mice at 12 h.p.o. ($n = 4$) and 27 h.p.o. ($n = 4$) was purified using TRIzol reagent (Life Technologies) according to the manufacturer’s instructions. The purified total RNA (83.3 ng μL^{-1}) was used as a template to synthesise cDNA using ReverTra Ace qPCR RT Master Mix (Toyobo). Quantitative polymerase chain reaction (qPCR) analysis was performed on the cDNA (20 ng μL^{-1}) using THUNDERBIRD SYBR

qPCR Mix (Toyobo) and the following gene-specific primers (5′–3′): matrix metalloproteinase 2 (*Mmp2*), ACGATGATGACCGGAAGTG (forward) and AATCGGAAGTTCTTGGTGTAGG (reverse; product size 157 bp); matrix metalloproteinase 9 (*Mmp9*), CATTCGCGTGGATAAGGAG (forward) and GAAACTCACACGCCAGAAGA (reverse; product size 112 bp); tissue-specific inhibitor of metalloproteinase 1 (*Timp1*), TCTGGCATCCTCTTGTTGCT (forward) and ACTCTTCACTGCGGTTCTGG (reverse; product size 292 bp); and β-actin (*Actb*; used as a housekeeping gene), TGTTACCAACTGGGACGACA (forward) and GGGGTGTTGAAGGTCTCAAA (reverse). The qPCR cycling conditions were 95°C for 1 min, followed by 40 cycles of 95°C for 15 s and 60°C for 45 s. Primers were obtained from Sigma-Aldrich. The concentration of the template RNA used in the reverse transcription reaction was 83.3 ng μL^{-1}, whereas the concentration of cDNA used in the PCR reaction was 20.0 ng μL^{-1}. Data were normalised against the expression level of *Actb* and analysed using the $\Delta\Delta C_t$ method.

Statistical analysis

Results are expressed as the mean ± s.e.m. Non-parametric analyses were used to analyse the data. Data between two groups were compared using the Mann–Whitney *U*-test, with two-sided $P < 0.05$ considered significant. The Kruskal–Wallis test was used to compare data among three or more groups. Multiple comparisons were performed using Scheffé's method when significant differences were observed overall ($P < 0.05$).

Results

Morphological features of embryos obtained after IVF

After IVF of oocytes obtained from C57BL/6 and MRL/MpJ mice, different categories of embryos (i.e. fertilised, unfertilised, abnormal and dead) were observed, as shown in Fig. 2*a–g*.

Surprisingly, there were many dead embryos, characterised by oocyte deformation and cytolysis, were numerous in the MRL/MpJ group (Fig. 2*g*), but these were not observed in the C57BL/6 group.

Histological ovary sections were obtained from mice at –12 h.p.o., a time point when antral follicles are considered to be maturing for ovulation. In the antral follicles of MRL/MpJ mice, elongated or compacted oocytes were frequently observed, whereas regular round-shaped oocytes were found in the antral follicles of the C57BL/6 mice (Fig. 2*h*, *i*). As shown in Fig. 2*j*, the oocyte aspect ratio was significantly higher in MRL/MpJ than C57BL/6 mice (1.40 ± 0.04 vs 1.20 ± 0.02 respectively), indicating an altered oocyte morphology in the antral follicles of MRL/MpJ mice. b

Number of embryos obtained after IVF and the fertilisation rate in MRL/MpJ than C57BL/6 mice

After superovulation treatment, MRL/MpJ mice produced 71.0 ± 13.4 COCs, whereas C57BL/6 mice produced 26.8 ± 2.8 COCs (Fig. 3*a*). In C57BL/6 mice, the number of fertilised, unfertilised, abnormal and dead embryos was 12.8 ± 1.6 (47.7 ± 2.5% of the total collected embryos), 1.2 ± 0.4 (4.9 ± 1.5%), 12.8 ± 1.6 (47.4 ± 2.0%) and 0 (0%) respectively. In MRL/MpJ mice, these number of fertilised, unfertilised, abnormal and dead embryos was 11.6 ± 4.6 (16.6 ± 4.4%), 9.2 ± 2.2 (14.7 ± 5.1%), 17.2 ± 3.2 (24.7 ± 2.3%) and 33.0 ± 9.2 (43.9 ± 7.1%), respectively. The number of unfertilised and dead embryos was significantly larger in MRL/MpJ than C57BL/6 mice. Furthermore, the fertilisation rate was significantly lower in MRL/MpJ than C57BL/6 mice (52.3 ± 11.9% vs 90.7 ± 2.8% respectively; Fig. 3*b*).

Number of COCs obtained under a natural oestrus cycle or after PMSG treatment

Under a natural oestrous cycle without superovulation treatment, C57BL/6 and MRL/MpJ mice ovulated 10.3 ± 0.5 and 12.0 ± 0.9 COCs respectively, with no significant difference

between the two strains (Fig. 4*a*). Because in non-equine species PMSG stimulates not only follicular development, but also ovulation (Practice Committee of the American Society for Reproductive Medicine Birmingham Alabama 2008), we also counted the number of ovulated COCs following injection of PMSG. After a single PMSG injection, C57BL/6 and MRL/MpJ mice ovulated 9.5 ± 2.7 and 9.5 ± 2.5 COCs respectively, which did not differ significantly (Fig. 4*b*). In contrast, the number of ovulated COCs after hCG treatment was significantly higher in MRL/MpJ than C57BL/6 mice (16.8 ± 4.2 vs 2.5 ± 2.5 respectively; Fig. 4*c*).

Comparative sequence analysis of ovulation-related genes in C57BL/6 and MRL/MpJ mice

We hypothesised that mutations in genes associated with female hormones or their receptors may contribute to the high sensitivity of MRL/MpJ mice to hCG. Therefore, we compared the exome sequences of *Inha*, *Inhbb*, *Fshb*, *Acvr1*, *Acvr2a*, *Acvr2b*, *Lhb*, *Inhba*, *Gnrh1*, *Lhcgr*, *Fshr*, *Esr1*, *Esr2* and *Pgr* genes between the two strains (Table 1). Genetic variants were detected in the following genes in MRL/MpJ mice: *Acvr1* (one synonymous exon variant and six intron variants), *Acvr2b* (seven synonymous exon and 15 intron variants), *Gnrh1* (one intron variant and one variant in the 3′ untranslated region (UTR)), *Lhcgr* (one synonymous exon, 12 intron and two upstream region variants) and *Esr1* (two synonymous exon variants and 12 intron variants). In addition to nine intron variants and five synonymous exon variants, *Pgr* in MRL/MpJ mice had two non-synonymous exon variants. The first one exon variant was a missense variant in position 118 in the DNA sequence (TCG) causing the serine to be replaced with a threonine, yielding ACG in the DNA sequence (variant ID: rs16808507). The second exon variant in *Pgr* was also a missense variant, in position 252 in the DNA sequence (GGA), causing the glycine to be replaced with a glutamic acid, yielding GAA (variant ID: rs16808511). Representatively, mice of the AKR/J and NZB/BINJ strains also have these two non-synonymous variants in *Pgr* (Mouse Phenome Database; https://phenome.jax.org/, data

accessed 13 Apr 2018). The number of embryos produced from the AKR/J and NZB/BINJ strains after superovulation treatment has been reported to be approximately 20 and 10 respectively (Spearow 1988; Yokoyama and Hioki 1990), indicating that it is unlikely that these variants cause the ovulation of high number of embryos in mice.

No variants were detected in the *Inha*, *Inhbb*, *Acvr2a*, *Fshb*, *Lhb*, *Inhba*, *Fshr* and *Esr2* genes. Thus, no coding region mutations affecting protein structure were identified in the genes examined.

Folliculogenesis and luteinisation after superovulation treatment

We examined ovarian histology after superovulation (Fig. 5*a–j*). At –12 h.p.o., just before ovulation, numerous antral follicles were observed and CL occupied the remaining space of the ovaries in both C57BL/6 and MRL/MpJ mice (Fig. 5*a*, *f*). At 12 h.p.o., ruptured follicles and corpora haemorrhagica were detected, and several antral follicles and CL were observed in both strains (Fig. 5*b*, *g*). At 18 and 36 h.p.o., some corpora haemorrhagica remained, and several CL were observed in the ovaries of C57BL/6 mice (Fig. 5*c*, *d*). In contrast, in MRL/MpJ mice, the number of CL in the ovaries increased at 18 h.p.o. (Fig. 5*h*) compared with 12 h.p.o. (Fig. 5*g*). At 36 h.p.o., numerous CL occupied almost the whole ovary in MRL/MpJ mice (Fig. 5*i*). The CL in both strains consisted of fibroblasts, vascular endothelial cells and granulosa and theca lutein cells containing vacuoles (Fig. 5*e*, *j*).

Next, we counted the number of antral follicles, ruptured follicles, corpora haemorrhagica and CL after superovulation in C57BL/6 and MRL/MpJ mice (Fig. 6*a*, *b*). In C57BL/6 mice, the number of antral follicles was significantly greater at –12 than at 12, 18 and 36 h.p.o. (15 ± 1 vs 5.1 ± 0.9, 5.0 ± 0.9 and 1.8 ± 0.8 respectively; $P < 0.05$). The number of ruptured follicles was significantly greater at 12 h.p.o. (10.0 ± 1.7) than at other time points (0.3 ± 0.3, 0.8 ± 0.5 and

0.3 ± 0.3 at –12, 18 and 36 h.p.o. respectively; $P < 0.05$) and the number of corpora haemorrhagica were significantly greater at 18 and 36 h.p.o. (14.0 ± 2.7 and 9.0 ± 1.5 respectively) than at –12 and 12 h.p.o. (0.3 ± 0.3 and 0.7 ± 0.4 respectively). However, the number of CL did not change significantly throughout the observation period (8.5 ± 1.6, 13.4 ± 1.8, 10.8 ± 2.9 and 9.5 ± 2.3 at –12, 12, 18 and 36 h.p.o. respectively).

Similar to C57BL/6 mice, the number of antral follicles in the MRL/MpJ strain was significantly greater at –12 h.p.o. (66.0 ± 4.9) than at other time points, and significantly greater at 12 and 18 than at 36 h.p.o. (22.0 ± 2.3 and 26.5 ± 1.9 vs 4.5 ± 2.5 respectively; $P < 0.05$). The number of ruptured follicles was significantly greater at 12 h.p.o. (21.0 ± 0.9) than at other time points, and significantly greater at 18 than at –12 and 36 h.p.o. (9.5 ± 1.8 vs 0 ± 0 and 0 ± 0 respectively; $P < 0.05$). However, unlike C57BL/6 mice, in MRL/MpJ mice there number of CL was significantly greater at 36 than at 12 h.p.o. (37.3 ± 6.1 vs 16.7 ± 1.2 respectively; $P < 0.05$).

The percentage of antral follicles, ruptured follicles, corpora haemorrhagica and CL relative to the total number of observed structures is shown in Fig. 6*c*, *d*. At –12 h.p.o., percentages were similar in the MRL/MpJ and C57BL/6 groups. At 12 h.p.o., the ovaries of MRL/MpJ mice had a significantly higher percentage of corpora haemorrhagica and a lower percentage of CL than in C57BL/6 mice. At 18 h.p.o., the percentage of antral follicles and ruptured follicles was significantly higher, whereas the percentage of corpora haemorrhagica was lower in ovaries of MRL/MpJ than C57BL/6 mice. Importantly, at 36 h.p.o., the percentage of corpora haemorrhagica was significantly lower and the percentage of CL was significantly higher in MRL/MpJ than C57BL/6 mice ($P < 0.05$). These data indicate differences in ovarian phenotypes between C57BL/6 and MRL/MpJ mice; in particular, there is an accelerated luteinisation in the latter strain.

Expression of MMPs and TIMPs in ovaries during luteinisation

MMPs and TIMPs play a key role in the breakdown of extracellular matrix (ECM) for luteinisation (Woessner 1991; Stocco *et al*. 2007). Among the MMP family of proteins, Mmp2 and Mmp9 appear to be important for luteinisation (Stocco *et al*. 2007). Our findings (Fig. 6*d*) suggest that ovaries of MRL/MpJ mice are forming CL most actively between 18 and 36 h.p.o. Therefore, we examined the expression of *Mmp2*, *Mmp9* and *Timp1* in ovaries of C57BL/6 and MRL/MpJ mice at 12 h.p.o. (before luteinisation) and at 27 h.p.o. (during luteinisation; Fig. 7). The expression of *Mmp2* and *Mmp9* did not change in either strain between 12 and 27 h.p.o., whereas *Timp1* expression was significantly lower at 27 than at 12 h.p.o. in MRL/MpJ mice (Fig. 7*a*). *Mmp9* expression at 12 h.p.o. was significantly lower in MRL/MpJ than C57BL/6 mice ($P < 0.05$). The ratio of *Mmp2* and *Mmp9* expression relative to that of *Timp1* increased significantly at 27 h.p.o. compared with 12 h.p.o. in MRL/MpJ mice (Fig. 7*b*).

In addition, we compared the exome sequences of *Mmp2*, *Mmp9* and *Timp1* (Table 2). No variants were detected in *Timp1*. *Mmp2* in MRL/MpJ mice had 18 synonymous exon variants, 47 intron variants and one variant in the 5′UTR. *Mmp9* in MRL/MpJ mice had one non-synonymous exon variant, which was a missense variant in position 639 in the DNA sequence (CTC) in which leucine was replaced with proline, yielding CCC in the DNA sequence (variant ID: rs13475086). AKR/J and BALB/cJ mice also harbour this non-synonymous variant in *Mmp9* (Mouse Phenome Database; https://phenome.jax.org/, data accessed 13 Apr 2018). These strains of mice exhibit slower healing than MRL/MpJ mice (Li *et al*. 2001), indicating that it is unlikely that this variant causes the faster luteinisation related to the faster healing in MRL/MpJ mice.

Discussion

Consistent with our previous findings (Hosotani *et al*. 2018) and other reports (Yokoyama and Hioki 1990), in this study MRL/MpJ mice ovulated significantly more COCs than did C57BL/6 mice after superovulation treatment. MRL/MpJ mice generated approximately 70 oocytes after the injection of PMSG and hCG, and approximately 10 oocytes in the normal oestrous cycle. These results indicate that the MRL/MpJ strain has a higher sensitivity to these gonadotrophin treatments than does the C57BL/6 strain. In equines, PMSG is known as the equine chorionic gonadotrophin and shows only LH-like activity (Practice Committee of the American Society for Reproductive Medicine Birmingham Alabama 2008). However, in non-equine species, PMSG shows both FSH and LH activity, and thus stimulates not only folliculogenesis, but also ovulation and luteinisation (Practice Committee of the American Society for Reproductive Medicine Birmingham Alabama 2008). A previous study discussed the possibility that ovulated oocytes induced by PMSG treatment remained in the oviducts until subsequent ovulation following injection of hCG (Yokoyama and Hioki 1990). However, in the present study the number of ovulated COCs following PMSG treatment was almost equal between the MRL/MpJ and C57BL/6 strains, and comparable to that of COCs under the natural oestrous cycle. This is consistent with the findings of another study that compared the number of ovulated oocytes after PMSG injection with that ovulated in normal oestrus (Kaufman and Whittingham 1972). Interestingly, MRL/MpJ mice produced more COCs than did C57BL/6 mice after a single injection of hCG. However, the total number of COCs generated following injection of either PMSG or hCG alone did not reach the number generated after sequential injections of PMSG and hCG. Therefore, both hCG and sequential injections of PMSG and hCG have stronger effects on ovulation in MRL/MpJ than C57BL/6 mice. Based on these findings, we hypothesised that mutations in genes associated with female hormones and their

receptors contributed to the high sensitivity to hCG observed in the MRL/MpJ strain. However, comparison of the exon sequences of several such genes (*Inha*, *Inhbb*, *Fshb*, *Acvr1*, *Acvr2a*, *Acvr2b*, *Lhb*, *Inhba*, *Gnrh*, *Lhcgr* and *Fshr*) between the C57BL/6 and MRL/MpJ strains found no coding region variants predicted to affect protein structure and function. Therefore, the superovulation-related phenotype in MRL/MpJ mice may be related to an altered expression of these genes in the ovary and/or in other organs associated with the hypothalamic–pituitary–gonadal axis, which could arise due to genetic variation in sequences outside of coding regions, such as in gene promoters.

Approximately 44% of embryos developed from ovulated oocytes in MRL/MpJ mice were dead, and the fertilisation rate was significantly lower for the MRL/MpJ than C57BL/6 strain. These results indicate the low quality of ovulated oocytes in MRL/MpJ mice. Various factors, such as genes, hormone levels, chemical interactions and environment and physical conditions, affect oocyte quality (Mermillod *et al*. 2008; Revelli *et al*. 2009; Sirotkin 2010; Carpintero *et al*. 2014). Importantly, previous studies reported that the percentage of cells undergoing apoptosis in cumulus cells increased in oocytes within follicles subjected to hydrostatic pressure (Rashidi *et al*. 2014). Our histological observations revealed a more elongated oocyte morphology in MRL/MpJ than C57BL/6 mice. It is not clear whether this morphological change is due to factors intrinsic to oocytes or whether it is influenced by the microenvironment, such as by pressure from the large number of developing follicles in MRL/MpJ mice. Because ovaries in MRL/MpJ mice contain a larger number of follicles than ovaries in C57BL/6 mice, it is possible that the poorer oocyte quality in MRL/MpJ mice results from exposure to high pressure. We did not observe the morphological abnormality in embryos *in vitro*. Furthermore, the *in vitro* fertilisation rate of human ovoid embryos is not affected, but delayed preimplantation development is seen (Ebner *et al*. 2008). There are no reports regarding how an ovoid shape of

oocytes in ovarian sections can affect the fertilisation rate and oocyte quality. However, the data suggest the possibility that an excessive number of follicles in an ovary can affect the oocyte quality in multifetal animals such as mice.

The folliculogenesis pattern was similar in MRL/MpJ and C57BL/6 mice before ovulation and the injection of hCG, with antral follicles accounting for most follicles in the ovary. After ovulation, MRL/MpJ mice formed CL within 36 h, whereas corpora haemorrhagica were numerous in C57BL/6 mice even after 36 h. These results indicate that the differentiation of ovulated follicles to CL occurs faster in MRL/MpJ than C57BL/6 mice. In addition, the higher percentage of ruptured follicles at 18 h.p.o. in MRL/MpJ than C57BL/6 mice indicates that ovulation from matured follicles continues for a longer period in MRL/MpJ than C57BL/6 mice, which may be due to the high sensitivity of the former strain to artificial ovulation.

In a previous study (Hosotani *et al*. 2018), we considered that the accelerated luteinisation in MRL/MpJ mice would be associated with the enhanced healing ability in this strain. Several possible explanations for the enhanced healing capacity of MRL/MpJ mice have been proposed, including cell cycle and proliferative features, increased stem cell quantity and/or quality and enhanced immune response (Heydemann 2012). In particular, changes in the ECM regulated by MMPs appeared to be crucial for the healing capacity of the MRL/MpJ strain (Heydemann 2012). ECM remodelling is cooperatively and tightly regulated by interactions between proteases and their inhibitors, such as MMPs and TIMPs respectively (Woessner 1991). For example, it was proposed that neutrophils and macrophages within wounds secrete significantly higher amounts of active MMP-2 and MMP-9 and lower amounts of TIMPs in MRL/MpJ than C57BL/6 mice (Gourevitch *et al*. 2003; Heydemann 2012). Importantly, in the CL, a transient endocrine gland, marked morphological changes are found upon the differentiation of luteal cells, and this process also involves changes in the ECM that enable cell migration and

neovascularisation in the newly formed CL (Davis and Rueda 2002; Stocco *et al*. 2007). Within the MMP family of proteins, MMP-2 and MMP-9 appear to be important for luteinisation (Stocco *et al*. 2007). The ratio of active MMPs to TIMPs may be important in maintaining an ECM microenvironment conducive to the differentiation of follicle-derived cells into luteal cells (Smith *et al*. 1999). Our results showed that the ratio of *Mmp2* and *Mmp9* to *Timp1* was elevated earlier in MRL/MpJ than C57BL/6 mice, resulting in the MMP–TIMP balance shifting towards MMP shortly after ovulation in MRL/MpJ mice. This suggests that accelerated ECM remodelling, as observed in wound healing, also occurs in the ovulated and ruptured follicles in MRL/MpJ mice, leading to quick luteinisation. In addition, oocyte development during nest breakdown and folliculogenesis is accelerated in neonatal MRL/MpJ mice (Yamashita *et al*. 2015), and this strain has a high frequency of ovarian cysts at older ages (Kon *et al*. 2007; Lee *et al*. 2011). Together, these results indicate that the MRL/MpJ mice have unique phenotypes associated with the female reproductive system throughout life.

In conclusion, the matured MRL/MpJ strain has unique phenotypes in female reproductive function, such as high sensitivity to gonadotrophin treatment and a faster process of luteinisation; these characteristics can contribute to the study of the mechanism of follicle remodelling and female reproductive function.

Conflicts of interest

The authors declare no conflicts of interest.

Acknowledgements

This work was supported, in part, by the Hokkaido University Tenure Track Program (Y. H. A. Elewa) and the Program for Leading Graduate Schools (Hokkaido University) from the Japanese Ministry of Education, Culture, Sports, Science and Technology (M. Hosotani). The research described in this paper

was presented, in part, at the 159th Japanese Association of Veterinary Anatomists, 6–8 September 2016, Kanagawa, Japan, at the 160th Japanese Association of Veterinary Anatomists, 15 September 2017, Kagoshima, Japan, and at the 6th Congress of Asian Association of Veterinary Anatomists, 15–16 October 2017, Kuching, Malaysia.

References

Buhimschi, C. S., Zhao, G., Sora, N., Madri, J. A., Buhimschi, I. A., Allsworth, J., Stevens, E., Macones, G., Buhimschi, C., and Weiner, C. (2010). Myometrial wound healing post-cesarean delivery in the MRL/MpJ mouse model of uterine scarring. *Am. J. Pathol.* **177**, 197–207 doi:10.2353/ajpath.2010.091209.

Carpintero, N. L., Suárez, O. A., Mangas, C. C., Varea, C. G., and Rioja, R. G. (2014). Follicular steroid hormones as markers of oocyte quality and oocyte development potential. *J. Hum. Reprod. Sci.* **7**, 187–193 doi:10.4103/0974-1208.142479.

Clark, L. D., Clark, R. K., and Heber-Katz, E. (1998). A new murine model for mammalian wound repair and regeneration. *Clin. Immunol. Immunopathol.* **88**, 35–45 doi:10.1006/clin.1998.4519.

Davis, J. S., and Rueda, B. R. (2002). The corpus luteum: an ovarian structure with maternal instincts and suicidal tendencies. *Front. Biosci.* **7**, 1949–1978 doi:10.2741/davis1.

Ebner, T., Shebl, O., Moser, M., Sommergruber, M., and Tews, G. (2008). Developmental fate of ovoid oocytes. *Hum. Reprod.* **23**, 62–66 doi:10.1093/humrep/dem280.

Gourevitch, D., Clark, L., Chen, P., Seitz, A., Samulewicz, S. J., and Heber-Katz, E. (2003). Matrix metalloproteinase activity correlates with blastema formation in the regenerating MRL mouse ear hole model. *Dev. Dyn.* **226**, 377–387 doi:10.1002/dvdy.10243.

Heydemann, A. (2012). The super super-healing MRL mouse strain. *Front. Biol. (Beijing)* **7**, 522–538 doi:10.1007/s11515-012-1192-4.

Hosotani, M., Ichii, O., Nakamura, T., Kanazawa, S. O., Elewa, Y. H. A., and Kon, Y. (2018). Autoimmune abnormality affects ovulation and oocyte-pick-up in MRL/MpJ-Fas$^{lpr/lpr}$ mice. *Lupus* **27**, 82–94 doi:10.1177/0961203317711772.

Ichii, O., Konno, A., Sasaki, N., Endoh, D., Hashimoto, Y., and Kon, Y. (2008). Autoimmune glomerulonephritis induced in congenic mouse strain carrying telomeric region of chromosome 1 derived from MRL/MpJ. *Histol. Histopathol.* **23**, 411–422 doi:10.14670/HH-23.411.

Kaufman, M. H., and Whittingham, D. G. (1972). Viability of mouse oocytes ovulated within 14 hours of an injection of pregnant mares' serum gonadotrophin. *J. Reprod. Fertil.* **28**, 465–468 doi:10.1530/jrf.0.0280465.

Kon, Y., and Endoh, D. (2000). Morphological study of metaphase-specific apoptosis in MRL mouse testis. *Anat. Histol. Embryol.* **29**, 313–319 doi:10.1046/j.1439-0264.2000.00279.x.

Kon, Y., Konno, A., Hashimoto, Y., and Endoh, D. (2007). Ovarian cysts in MRL/MpJ mice originate from rete ovarii. *Anat. Histol. Embryol.* **36**, 172–178 doi:10.1111/j.1439-0264.2006.00728.x.

Lee, S.-H., Ichii, O., Otsuka, S., Yaser Hosney, E., Namiki, Y., Hashimoto, Y., and Kon, Y. (2011). Ovarian cysts in MRL/MpJ mice are derived from the extraovarian rete: a developmental study. *J. Anat.* **219**, 743–755 doi:10.1111/j.1469-7580.2011.01431.x.

Leferovich, J. M., Bedelbaeva, K., Samulewicz, S., Zhang, X. M., Zwas, D., Lankford, E. B., and Heber-Katz, E. (2001). Heart regeneration in adult MRL mice. *Proc. Natl Acad. Sci. USA* **98**, 9830–9835 doi:10.1073/pnas.181329398.

Li, X., Gu, W., Masinde, G., Hamilton-Ulland, M., Xu, S., Mohan, S., and Baylink, D. J. (2001). Genetic control of the rate of wound healing in mice. *Heredity* **86**, 668–674 doi:10.1046/j.1365-2540.2001.00879.x.

Mermillod, P., Dalbis-Tran, R., Uzbekova, S., Thlie, A., Traverso, J.-M., Perreau, C., Papillier, P., and Monget, P. (2008). Factors affecting oocyte quality: who is driving the follicle? *Reprod. Domest. Anim.* **43**, 393–400 doi:10.1111/j.1439-0531.2008.01190.x.

Nakamura, T., Sakata, Y., Otsuka-Kanazawa, S., Ichii, O., Chihara, M., Nagasaki, K., Namiki, Y., and Kon, Y. (2014). Genomic analysis of the appearance of ovarian mast cells in neonatal MRL/MpJ mice. *PLoS One* **9**, e100617. doi:10.1371/journal.pone.0100617

Otsuka, S., Konno, A., Hashimoto, Y., Sasaki, N., Endoh, D., and Kon, Y. (2008). Oocytes in newborn MRL mouse testes. *Biol. Reprod.* **79**, 9–16 doi:10.1095/biolreprod.107.064519.

Practice Committee of the American Society for Reproductive Medicine, Birmingham, Alabama. (2008). Gonadotropin preparations: past, present, and future perspectives. *Fertil. Steril.* **90**(Suppl.), S13–S20 doi:10.1016/j.fertnstert.2008.08.031.

Rashidi, Z., Azadbakht, M., Amini, A., and Karimi, I. (2014). Hydrostatic pressure affects *in vitro* maturation of oocytes and follicles and increases granulosa cell death. *Cell J.* **15**, 282–293.

Revelli, A., Delle Piane, L., Casano, S., Molinari, E., Massobrio, M., and Rinaudo, P. (2009). Follicular fluid content and oocyte quality: from single biochemical markers to metabolomics. *Reprod. Biol. Endocrinol.* **7**, 40 doi:10.1186/1477-7827-7-40.

Santiago-Raber M.-L., Laporte C., Reininger L., and Izui S. (2004). Genetic basis of murine lupus. *Autoimmun. Rev.* **3**, 33–39. doi:10.1016/S1568-9972(03)00062-4

Shiozuru, D., Ichii, O., Kimura, J., Nakamura, T., Elewa, Y. H. A., Otsuka-Kanazawa, S., and Kon, Y. (2016). MRL/MpJ mice show unique pathological features after experimental kidney injury. *Histol. Histopathol.* **31**, 189–204.

Sirotkin, A. V. (2010). Effect of two types of stress (heat shock/high temperature and malnutrition/serum deprivation) on porcine ovarian cell functions and their response to hormones. *J. Exp. Biol.* **213**, 2125–2130 doi:10.1242/jeb.040626.

Smith, M. F., McIntush, E. W., Ricke, W. A., Kojima, F. N., and Smith, G. W. (1999). Regulation of ovarian extracellular matrix remodelling by metalloproteinases and their tissue inhibitors: effects on follicular development, ovulation and luteal function. *J. Reprod. Fertil. Suppl.* **54**, 367–381.

Spearow, J. L. (1988). Major genes control hormone-induced ovulation rate in mice. *J. Reprod. Fertil.* **82**, 787–797 doi:10.1530/jrf.0.0820787.

Stocco, C., Telleria, C., and Gibori, G. (2007). The molecular control of corpus luteum formation, function, and regression. *Endocr. Rev.* **28**, 117–149 doi:10.1210/er.2006-0022.

Takeo, T., and Nakagata, N. (2010). Combination medium of cryoprotective agents containing L-glutamine and methyl-β-cyclodextrin in a preincubation medium yields a high fertilization rate for cryopreserved C57BL/6J mouse sperm. *Lab. Anim.* **44**, 132–137 doi:10.1258/la.2009.009074.

Takeo, T., and Nakagata, N. (2011). Reduced glutathione enhances fertility of frozen/thawed C57BL/6 mouse sperm after exposure to methyl-beta-cyclodextrin. *Biol. Reprod.* **85**, 1066–1072 doi:10.1095/biolreprod.111.092536.

Takeo, T., Hoshii, T., Kondo, Y., Toyodome, H., Arima, H., Yamamura, K., Irie, T., and Nakagata, N. (2008). Methyl-beta-cyclodextrin improves fertilizing ability of C57BL/6 mouse sperm after freezing and thawing by facilitating cholesterol efflux from the cells. *Biol. Reprod.* **78**, 546–551 doi:10.1095/biolreprod.107.065359.

Woessner, J. F. (1991). Matrix metalloproteinases and their inhibitors in connective tissue remodeling. *FASEB J.* **5**, 2145–2154 doi:10.1096/fasebj.5.8.1850705.

Yamashita, Y., Nakamura, T., Otsuka-Kanazawa, S., Ichii, O., and Kon, Y. (2015). Morphological characteristics observed during early follicular development in perinatal MRL/MpJ mice. *Jpn. J. Vet. Res.* **63**, 25–36 doi:10.14943/jjvr.63.1.25.

Yokoyama, M., and Hioki, K. (1990). The copulation rate and the embryo recovery rate following induced superovulation in various strains of mice. *J. Mamm. Ova Res.* **7**, 89–94 doi:10.14893/jmor1984.7.89.

Fig. 1. The superovulation treatment protocol used in the present study. Mice were injected with pregnant mare's serum gonadotrophin (PMSG) intraperitoneally; 48 h after PMSG injection, defined as –12 h postovulation (h.p.o.), mice were injected intraperitoneally with human chorionic gonadotrophin (hCG) or had their ovaries removed. Ovaries were collected 24 h (12 h.p.o.), 30 h (18 h.p.o.), 39 h (27 h.p.o.) and 48 h (36 h.p.o.) after hCG injection.

Fig. 2. Morphological observations of embryos after IVF of oocytes obtained from superovulated C57BL/6 (*a*, *c*, *e*) and MRL/MpJ (*b*, *d*, *f*) mice. (*a*, *b*) Fertilised embryos that have two cells of the same size. (*c*, *d*) Unfertilised embryos. (*e*, *f*) Abnormal cleavage in embryos, which have either three or more cells or two cells of different sizes. (*g*) Dead embryos derived from MRL/MpJ mice that have a large cytoplasm and condensed cells. (*h*, *i*) Morphological differences between oocytes contained in antral follicles at –12 h.p.o. in C57BL/6 and MRL/MpJ mice. Scale bars = 50 μm. (*j*) The oocyte aspect ratio (maximum diameter/minimum diameter) in C57BL/6 mice ($n = 4$; 13–15 oocytes analysed in each ovary) and MRL/MpJ mice ($n = 4$; 40–61 oocytes analysed in each ovary). Data are the mean ± s.e.m. $^*P < 0.05$ (Mann–Whitney *U*-test).

Fig. 3. Results of the fertilisation assay in embryos obtained from superovulated C57BL/6 and MRL/MpJ mice. (*a*) Number of different types of embryos generated per mouse through IVF. Data are the mean ± s.e.m. ($n = 5$ in each strain). *$P < 0.05$ (Mann–Whitney *U*-test). †$P < 0.05$ compared with the same embryo type in C57BL/6 mice (Mann–Whitney *U*-test). (*b*) Fertilisation rate calculated from the number of fertilised and unfertilised embryos shown in (*a*). Data are the mean ± s.e.m. ($n = 5$ in each strain). *$P < 0.05$ (Mann–Whitney *U*-test).

Fig. 4. Number of cumulus–oocyte complexes (COCs) produced (*a*) under a natural oestrous cycle and after injection of (*b*) pregnant mare's serum gonadotrophin (PMSG) or (*c*) human chorionic gonadotrophin (hCG). Data are the mean ± s.e.m. ($n = 5$ in each strain for (*a*); $n = 4$ in each strain for (*b*) and (*c*)). There were no significant differences in the number of COCs ovulated between C57BL/6 and MRL/MpJ mice under a natural oestrous cycle or after injection of PMSG. *$P < 0.05$ (Mann–Whitney *U*-test).

Fig. 5. Ovarian histology before and after superovulation in C57BL/6 and MRL/MpJ mice. CL, corpus luteum; h.p.o., h postovulation. The squares indicated in (*d*) and (*i*) are magnified in (*e*) and (*j*) respectively, with insets showing lutein cells containing vacuoles. Arrows indicate antral follicles, arrowheads indicate ruptured follicles, daggers indicate corpora haemorrhagica and asterisks indicate corpora lutea. Scale bars = 300 µm (*a–d*, *f–i*); 50 µm (*e*, *j*).

Fig. 6. (*a*, *b*) Number and (*c*, *d*) percentage of ovarian follicle-related structures in superovulated C57BL/6 (*a*, *c*) and MRL/MpJ (*b*, *d*) mice. Data are the mean ± s.e.m. of ovaries from four mice in each group at –12, 18 and 36 h postovulation (h.p.o.) and six mice in each group at 18 h.p.o. Asterisks indicate significant differences compared with the other three time points within the same strain are shown. Significant differences –12, 12 and 36 h.p.o. within the same strain are indicated as '–12', '12' and '36' respectively ($P < 0.05$, Kruskal–Wallis test followed by Scheffé's test). In (*d*), the daggers indicate

significant differences in the same structure compared with the C57BL/6 strain ($P < 0.05$, Mann–Whitney *U*-test).

Fig. 7. (*a*) Expression of matrix metalloproteinase 2 (*Mmp2*), matrix metalloproteinase 9 (*Mmp9*) and tissue-specific inhibitor of metalloproteinase 1 (*Timp1*) mRNA during luteinisation in ovaries of superovulated C57BL/6 and MRL/MpJ mice and (b) the ratio of matrix metalloproteinase (MMP) mRNA to *Timp1* expression, as determined by quantitative real-time polymerase chain reaction at 12 and 27 h postovulation (h.p.o.). Data are the mean ± s.e.m. ($n = 4$ for each strain at each time point). *$P < 0.05$ (Mann–Whitney *U*-test).

Table 1. Polymorphisms in ovulation-related genes detected between C57BL/6 and MRL/MpJ strains using next-generation sequencing

chr, chromosome; SNV, single nucleotide variant; *Acvr1*, activin A, type1; *Acv2b*, activin receptor IIB; *Gnrh1*, gonadotrophin-releasing hormone 1; *Lhcgr*, luteinising hormone/choriogonadotrophin receptor; *Pgr*, progesterone receptor; *Esr1*, oestrogen receptor 1; UTR, untranslated region

Gene	Chr	Location (bp)		Strains		Region	Change	Variant ID
	no.	Start	End	C57BL/6	MRL/MpJ			
Acvr1	chr02	58448495	58448495	A	G	Intron	–	rs214065797
		58458835	58458835	G	T	Intron	–	rs230650639
		58458868	58458868	T	C	Intron	–	rs246215171
		58463020	58463020	T	C	Exon	Synonymous SNV	rs33549343
		58463229	58463229	G	A	Intron	–	rs228629097
		58477571	58477571	A	G	Intron	–	rs27909412
		58500669	58500669	C	A	Intron	–	rs261538744
Acvr2b	chr09	119427385	119427385	A	G	Intron	–	rs45872254
		119427427	119427431	TGCTC	–	Intron	–	-
		119427489	119427489	C	T	Exon	Synonymous SNV	rs254093865
		119427495	119427495	C	T	Exon	Synonymous SNV	rs245957907
		119427867	119427867	A	C	Intron	–	rs50502574
		119427874	119427874	A	G	Intron	–	rs214816821
		119427922	119427922	T	G	Intron	–	rs238044625
		119427962	119427962	C	T	Intron	–	rs48995394
		119428382	119428382	A	G	Exon	Synonymous SNV	rs220947222
		119428430	119428430	G	C	Exon	Synonymous SNV	rs236256586

		119428520	119428520	A	G	Exon	Synonymous SNV	rs30372811
		119428612	119428612	C	G	Intron	–	rs30134774
		119428620	119428620	G	–	Intron	–	-
		119429791	119429791	–	A	Intron	–	-
		119429811	119429811	G	A	Intron	–	rs249216178
		119429889	119429889	C	A	Exon	Synonymous SNV	rs50269096
		119429928	119429928	T	C	Exon	Synonymous SNV	rs231454902
		119430037	119430037	G	A	Intron	–	rs215251161
		119430059	119430059	A	G	Intron	–	rs50218863
		119430115	119430115	–	ATAGTCAGAATCGCCACGCC	Intron	–	-
		119430387	119430387	T	C	Intron	–	rs247262863
		119432888	119432888	A	–	Intron	–	-
Gnrh1	chr14	67746552	67746552	A	T	Intron	–	rs3023411
		67749359	67749359	A	–	3′UTR	–	-
Lhcgr	chr17	88765044	88765044	G	A	Exon	Synonymous SNV	rs45832892
		88765274	88765274	G	A	Intron	–	rs49175256
		88765283	88765283	T	C	Intron	–	rs49233045
		88765284	88765284	G	C	Intron	–	rs50445833
		88765297	88765297	A	G	Intron	–	rs50723996
		88765328	88765328	A	G	Intron	–	rs51548994
		88767223	88767223	–	C	Intron	–	-
		88767357	88767357	G	C	Intron	–	rs33145242
		88767384	88767384	A	C	Intron	–	rs33347120
		88769697	88769697	T	G	Intron	–	rs3717394
		88769748	88769748	T	A	Intron	–	rs3717517

		88769935	88769937	AAC	–	Intron	–	rs235138678
		88772141	88772141	G	A	Intron	–	rs52183165
		88792035	88792035	C	T	Upstream	–	rs52233715
		88792040	88792040	G	A	Upstream	–	rs52545123
Pgr	chr09	8900819	8900819	T	A	Exon	Non-synonymous SNV	rs16808507
		8900914	8900914	A	T	Exon	Synonymous SNV	rs222662569
		8900959	8900959	G	A	Exon	Synonymous SNV	rs246932498
		8901222	8901222	G	A	Exon	Non-synonymous SNV	rs16808511
		8901259	8901259	C	A	Exon	Synonymous SNV	rs16808515
		8901730	8901730	C	G	Exon	Synonymous SNV	rs16808520
		8922762	8922762	C	T	Intron	–	rs16808540
		8956132	8956132	–	TGT	Intron	–	–
		8956215	8956215	T	A	Intron	–	rs16808632
		8956228	8956228	T	–	Intron	–	rs16808634
		8956263	8956263	T	C	Exon	Synonymous SNV	rs16808635
		8956426	8956426	A	G	Intron	–	rs38678743
		8956474	8956474	G	A	Intron	–	rs253462664
		8956484	8956484	T	C	Intron	–	rs262156449
		8956517	8956517	A	C	Intron	–	rs216472569
		8956530	8956530	C	A	Intron	–	rs234992683
Esr1	chr10	4964668	4964668	G	A	Intron	–	rs29383782
		4964798	4964798	C	T	Intron	–	rs50779278
		4964883	4964883	T	G	Intron	–	rs49862291
		4964886	4964886	C	T	Intron	–	rs46991755
		4966154	4966154	G	T	Intron	–	rs29315913

	4966407	4966407	T	C	Intron	–	rs29330062
	4969082	4969082	A	G	Intron	–	rs16821149
	4969093	4969093	G	A	Intron	–	rs16821150
	4969094	4969094	T	A	Intron	–	rs16821151
	4969106	4969116	TGTCTTC GAGA	–	Intron	–	rs214903150
	4969210	4969210	G	T	Exon	Synonymous SNV	rs16821161
	4969249	4969249	A	T	Exon	Synonymous SNV	rs47715549
	4969307	4969307	C	T	Intron	–	rs46716572
	4969389	4969389	C	T	Intron	–	rs47973744

Table 2. Polymorphisms in luteinisation-related genes detected between the C57BL/6 and MRL/MpJ strains using next-generation sequencing

chr, chromosome; SNV, single nucleotide variant; *Mmp2*, matrix metalloproteinase 2; *Mmp9*: matrix metalloproteinase 9; UTR, untranslated region

Gene	Chr no.	Location (bp)		Strains		Region	Change	Variant ID
		Start	End	C57BL/6	MRL/MpJ			
Mmp2	chr08	92827509	92827509	C	G	5′UTR	–	rs50154992
		92827789	92827789	T	C	Intron	–	rs47915014
		92830595	92830595	A	G	Intron	–	rs50707366
		92830606	92830606	T	A	Intron	–	rs47202868
		92830632	92830632	C	T	Exon	Synonymous SNV	rs48669156
		92831599	92831602	GCAC	–	Intron	–	–
		92831611	92831611	G	A	Intron	–	rs52544499
		92831862	92831862	T	C	Intron	–	rs47205486
		92832757	92832757	A	G	Intron	–	rs45755812

92832783	92832783	A	G	Exon	Synonymous SNV	rs47346055
92832906	92832906	C	T	Intron	–	rs47940001
92832935	92832935	T	C	Intron	–	rs46642227
92832937	92832937	T	C	Intron	–	rs50670061
92832983	92832983	T	C	Intron	–	rs51535272
92833019	92833019	C	T	Intron	–	rs46335818
92833037	92833037	G	T	Intron	–	rs50714352
92833193	92833193	C	T	Exon	Synonymous SNV	rs46421166
92833273	92833273	C	T	Intron	–	rs51678138
92833286	92833286	T	C	Intron	–	rs45705750
92833302	92833302	T	C	Intron	–	rs50894680
92835871	92835871	A	G	Intron	–	rs45886546
92835887	92835887	A	G	Intron	–	rs46632834
92835925	92835925	T	A	Intron	–	rs47396275
92835947	92835947	T	C	Intron	–	rs48288639
92835950	92835950	C	A	Intron	–	rs45708441
92835961	92835961	C	–	Intron	–	–
92835994	92835994	A	T	Exon	Synonymous SNV	rs47334964
92836015	92836015	C	T	Exon	Synonymous SNV	rs50617380
92836072	92836072	T	C	Exon	Synonymous SNV	rs46039319
92836120	92836120	G	A	Exon	Synonymous SNV	rs50745645
92836132	92836132	T	C	Exon	Synonymous SNV	rs49465794
92836172	92836172	A	G	Intron	–	–
92836208	92836208	T	C	Intron	–	rs50106637
92836248	92836248	A	C	Intron	–	rs50508247

92837027	92837027	G	A	Exon	Synonymous SNV	rs33504743
92837149	92837149	T	C	Intron	–	rs46426201
92839119	92839119	T	C	Intron	–	rs50615049
92839341	92839341	G	T	Exon	Synonymous SNV	rs46885156
92839428	92839428	A	C	Intron	–	rs47250679
92840287	92840287	–	T	Intron	–	–
92840355	92840355	T	G	Intron	–	rs47524903
92840387	92840387	T	C	Intron	–	rs48300311
92840400	92840400	C	T	Exon	synonymous SNV	rs46870953
92840436	92840436	A	G	Exon	Synonymous SNV	rs51331853
92840440	92840440	C	T	Exon	Synonymous SNV	rs51553188
92840567	92840567	A	T	Intron	–	–
92840621	92840621	A	G	Intron	–	rs49727866
92843814	92843814	T	C	Intron	–	rs32814582
92844028	92844028	T	C	Intron	–	rs45701744
92846032	92846032	G	T	Intron	–	rs48669406
92846077	92846077	T	C	Intron	–	rs51010704
92846106	92846106	T	C	Exon	Synonymous SNV	rs46518220
92846109	92846109	T	C	Exon	Synonymous SNV	rs46528268
92846265	92846265	C	T	Intron	–	rs33044164
92846284	92846284	C	A	Intron	–	rs49358673
92846296	92846304	ATGTGGCTT	–	Intron	–	–
92846309	92846309	T	G	Intron	–	rs240469150
92846340	92846340	T	A	Intron	–	rs50419882
92846341	92846341	T	C	Intron	–	rs50984607

			92850078	92850078	G	A	Intron	–	rs46081866
			92850156	92850156	C	G	Exon	Synonymous SNV	rs49302213
			92850213	92850213	C	T	Exon	Synonymous SNV	rs48609021
			92850231	92850231	T	C	Exon	Synonymous SNV	rs51146338
			92852461	92852461	C	T	Intron	–	rs49769472
			92852477	92852477	A	G	Intron	–	rs46075410
			92852508	92852508	C	A	Intron	–	rs51124308
	Mmp9	chr02	164953375	164953375	T	C	Exon	Non-synonymous SNV	rs13475086

6

7

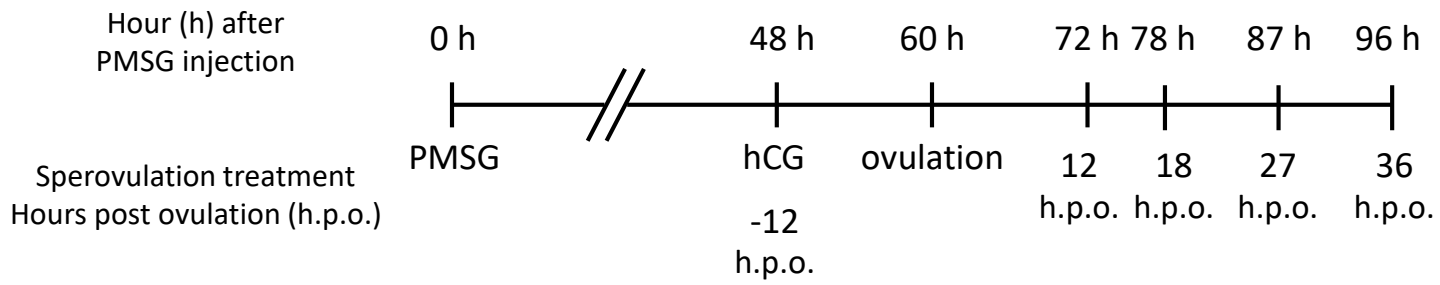
Hour (h) after PMSG injection
0 h
48 h
60 h
72 h
78 h
87 h
96 h
PMSG
hCG
ovulation
12 h.p.o.
18 h.p.o.
27 h.p.o.
36 h.p.o.
Sperovulation treatment
Hours post ovulation (h.p.o.)
-12 h.p.o.

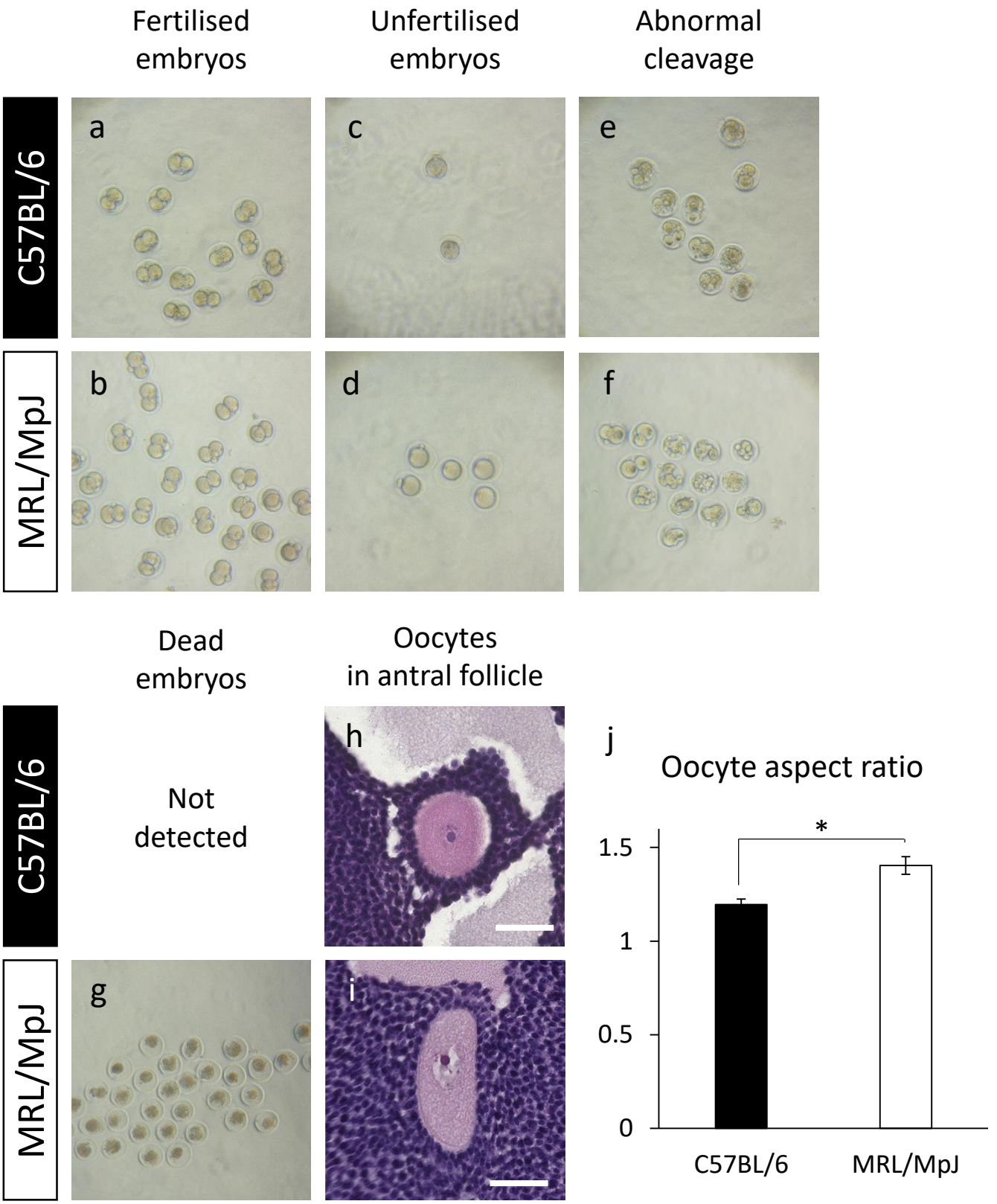
Fertilised embryos
Unfertilised embryos
Abnormal cleavage
C57BL/6
MRL/MpJ
a
b
c
d
e
f
Dead embryos
Oocytes in antral follicle
Not detected
h
g
i
j
Oocyte aspect ratio
*
1.5
1
0.5
0
C57BL/6
MRL/MpJ

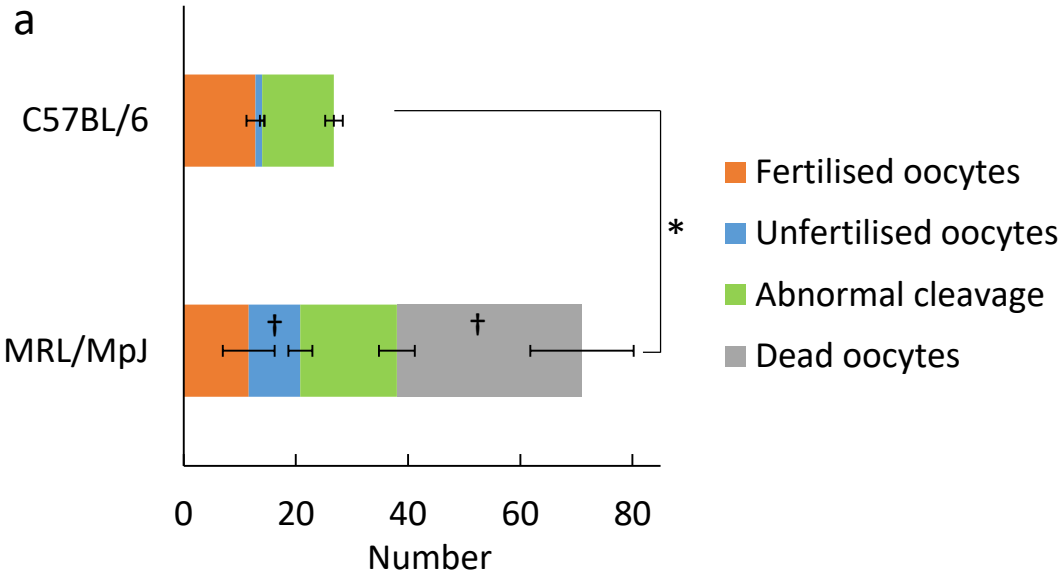
a
C57BL/6
MRL/MpJ
*
†
†
Fertilised oocytes
Unfertilised oocytes
Abnormal cleavage
Dead oocytes
0
20
40
60
80
Number

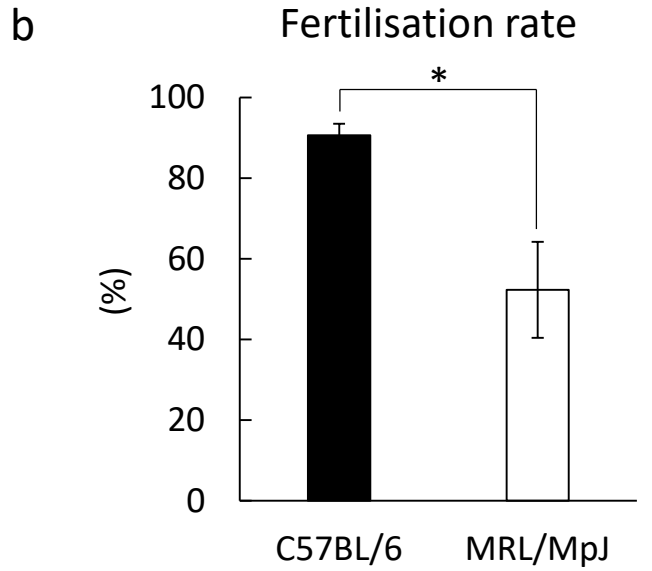
b
Fertilisation rate
*
100
80
60
40
20
0
(%)
C57BL/6
MRL/MpJ

a

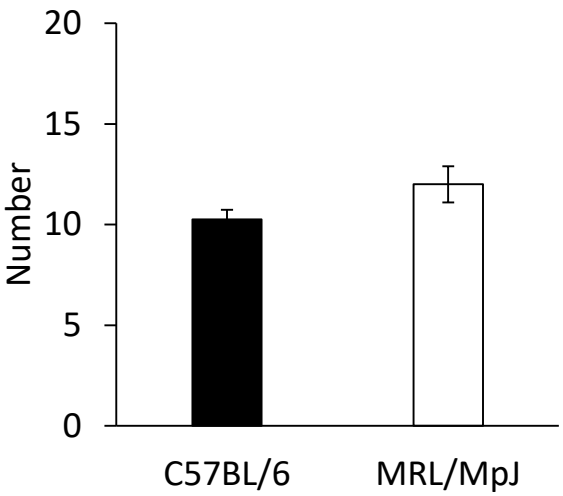
Naturally ovulated COCs
20
15
10
5
0
Number
C57BL/6
MRL/MpJ

b

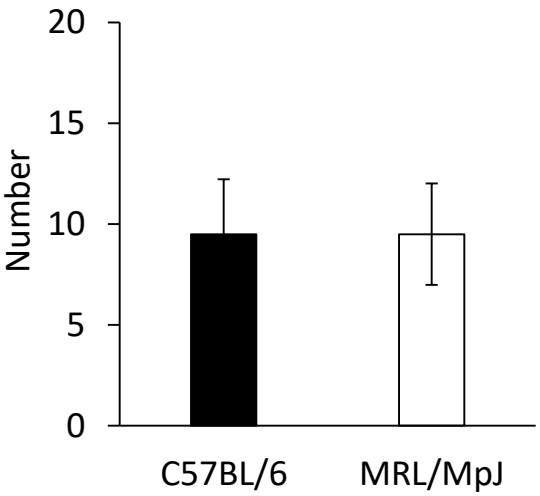
COCs ovulated by PMSG
20
15
10
5
0
Number
C57BL/6
MRL/MpJ

c

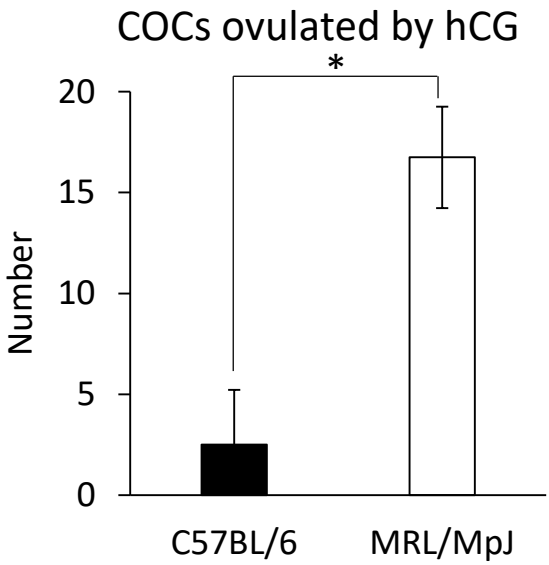
COCs ovulated by hCG
*
20
15
10
5
0
Number
C57BL/6
MRL/MpJ

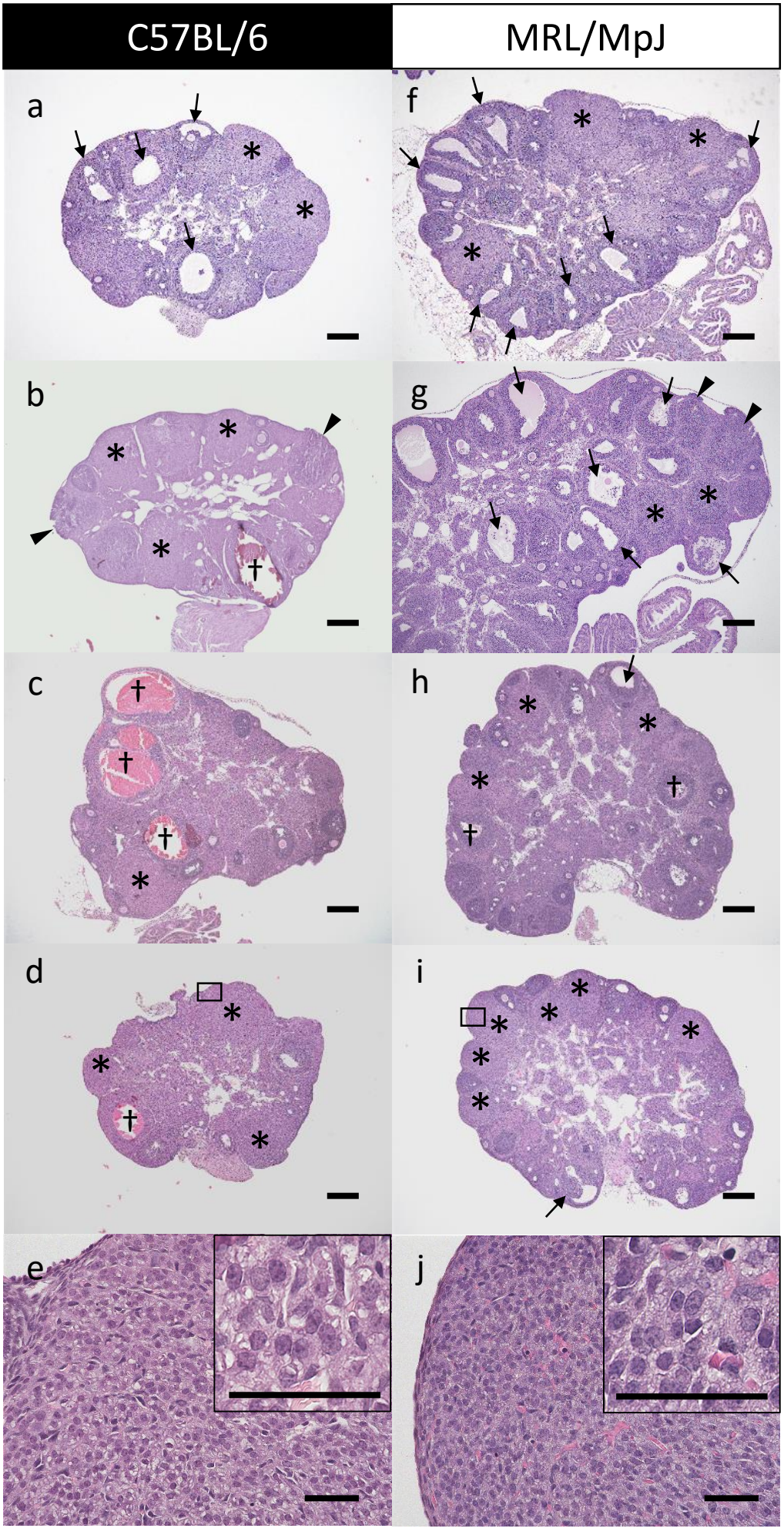
C57BL/6
MRL/MpJ
-12 h.p.o.
12 h.p.o.
18 h.p.o.
36 h.p.o.
CL
a
b
c
d
e
f
g
h
i
j

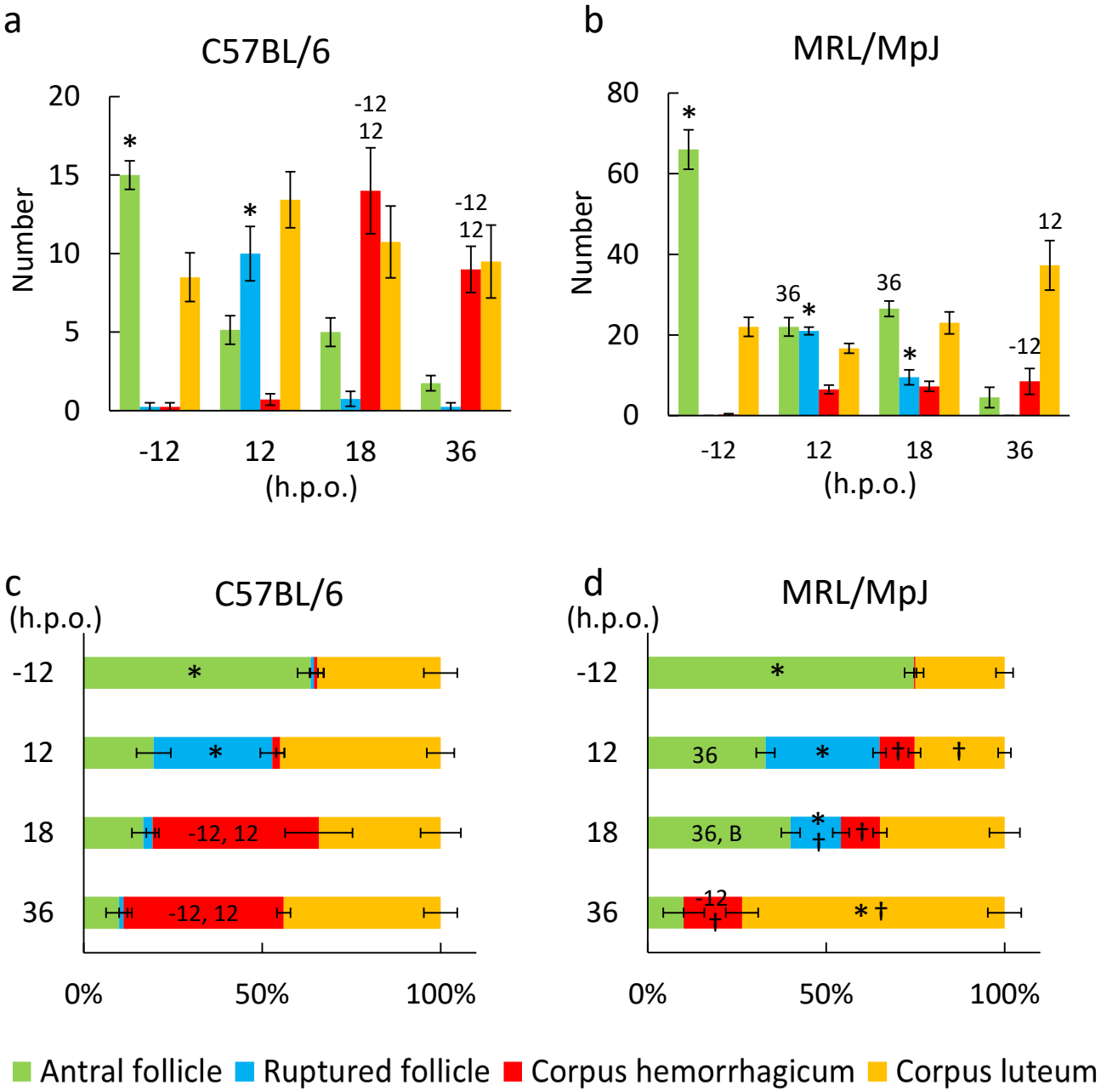
a
C57BL/6
Number
20
15
10
5
0
-12
12
18
36
(h.p.o.)
b
MRL/MpJ
Number
80
60
40
20
0
36
-12
12
(h.p.o.)
c
C57BL/6
(h.p.o.)
-12
12
18
36
-12, 12
0%
50%
100%
d
MRL/MpJ
(h.p.o.)
36, B
Antral follicle
Ruptured follicle
Corpus hemorrhagicum
Corpus luteum

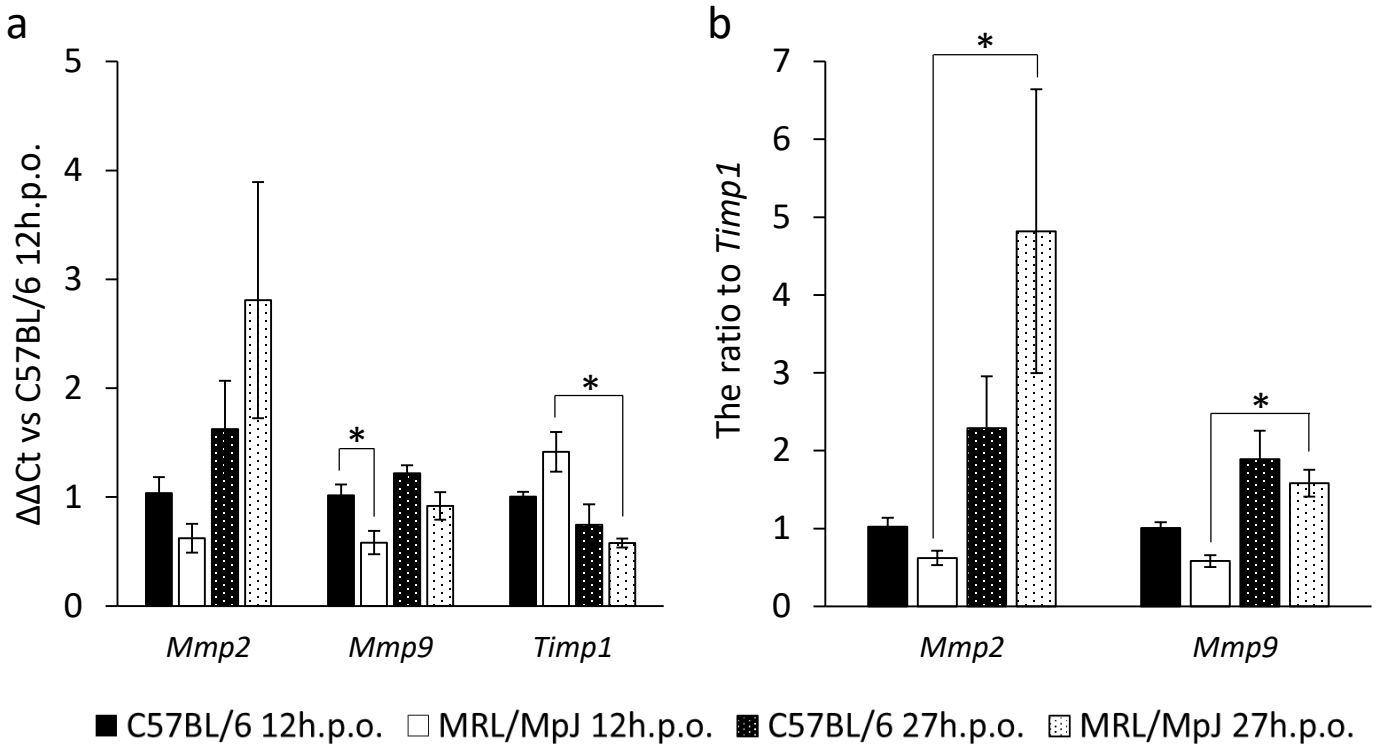
a
ΔΔCt vs C57BL/6 12h.p.o.
0
1
2
3
4
5
*
*
Mmp2
Mmp9
Timp1
b
The ratio to Timp1
0
1
2
3
4
5
6
7
*
*
Mmp2
Mmp9
C57BL/6 12h.p.o.
MRL/MpJ 12h.p.o.
C57BL/6 27h.p.o.
MRL/MpJ 27h.p.o.